Dual-Band Transceiver High Impedance Coil Array for Ultrahigh Field Magnetic Resonance Imaging

Masoud Sharifian Mazraeh Mollaei, Ali Sharifian Mazraeh Mollaei, and Constantin R. Simovski

***Abstract*— A novel approach for designing an element of an arrayed radio frequency coil for ultrahigh field magnetic resonance imaging (UHF MRI) is presented. The purpose of this approach is to achieve the dual-band transceiver regime in a compact array of magnetic antennas. Our work qualitatively develops the concept of the so-called high-impedance coil (HIC), combined with the adequate interfacing circuitry, which offers the decoupling of the HICs in the array due to the very high self-impedance compared to the mutual impedance. This concept has not been previously thought applicable to dual-band transceiver arrays. We show that, by slightly modifying only the cable shield, we achieve a dual-band transceiver high-impedance coil (dual-band TRHIC). The needed modification implies two asymmetric gaps granting two useful eigenmodes to the cable loop. The resonant excitation of these modes will allow the magnetic resonant scanning of both hydrogen and Phosphorus in the 7 T dc magnetic field. To verify our ideas, we simulated and measured a single TRHIC in both transmitting and receiving regimes and similarly studied two linear arrays made of two and three proposed TRHICs. The method of asymmetric gaps, in our opinion, allows one to engineer the targeted multifrequency operation of arrayed TRHICs decoupled at these frequencies.**

***Index Terms*— Decoupling of antennas, high-impedance coil (HIC), magnetic resonance imaging (MRI), shielded loop antennas, transceiver antenna.**

I. Introduction

FOR many years, phased array antennas have made the focus of research. Their magnetic resonance imaging (MRI) application where the arrayed radio frequency coils grant the enhancement of the spatial resolution and robustness of the scanned image has attracted the attention of many researchers. In what concerns, the antenna technique the main challenge is related to mutual coupling in these arrays. Coupling between the elements of these arrays results in the drastic reduction of efficiency due to the losses in the elements coupled to the reference one, in the high cross-talks distorting the useful signal, in the interchannel scattering and parasitic secondary near fields, in breaking the array operation, and, finally, in the critical decrease of signal-to-noise ratio (SNR) implying the erroneous image of the patient's organs (see [1]–[3]). Thus, the decoupling of antennas in these antenna arrays is a task of prime importance.

In case when the array is not compact, conventional methods of decoupling, such as inserting absorbing or reflecting compartment shields in the gaps between the elements, may be employed. However, when the volume of the antenna array is restricted and the gaps between the neighboring antennas are much smaller than both wavelengths and the element dimensions, other methods of decoupling are required [4]. Sometimes, in these cases, one uses an adaptive active circuitry compensating the parasitic electromotive forces (EMFs) induced by the neighboring antennas. However, adaptive technical solutions are very expensive that hinders their commercial applications [5]. In civil applications, different inexpensive methods have been introduced to decouple the tightly packed antennas in an array. In the following, we consider only those methods of decoupling, which are suitable for our targeted application–arrayed radio frequency coils for ultrahigh field magnetic resonance imaging (UHF MRI). In our case, each array element is a magnetic-type antenna that corresponds to its own channel of transmitting the primary pulses and receiving the echo signals. Note that several elements are necessary for obtaining high image resolution, whereas the volume of the array is always restricted by the MRI bore and sometimes by the requirement of minimal distance to the inspected part of the body (see [1]–[3] and [6]–[9]).

The most common way to decouple the loop antennas and simultaneously achieve the ultimate compactness of the array is to partially overlap the neighboring elements. For two intersecting loops, the mutual inductance can be nullified because the mutual inductance of two coplanar loops is negative and that of two coaxial loops is positive. However, this technique is applicable only in the case when the operation frequency lies in the quasi-static region of an antenna. In UHF MRI, the main operational band should cover the Larmor frequency of hydrogen (298 MHz). To be efficient, a loop antenna should be large enough with respect to the operation wavelength; to obtain good radiation efficiency at 298 MHz, the diameter should be of the order of 10–15 cm. Such a current loop at this frequency is not a pure magnetic dipole, and the mutual coupling of the adjacent array elements is not anymore purely inductive. Moreover, in this frequency band, the radiation is higher than in the bands corresponding to traditional MRI schemes. In this situation, one has to decouple not only adjacent loop antennas but also nonadjacent antennas. Thus,

Manuscript received January 8, 2021; revised June 30, 2021; accepted July 15, 2021. Date of publication September 15, 2021; date of current version February 3, 2022. *(Corresponding author: Masoud Sharifian Mazraeh Mollaei.)*

Masoud Sharifian Mazraeh Mollaei and Constantin R. Simovski are with the Department of Electronics and Nanoengineering, Aalto University, 02150 Espoo, Finland (e-mail: masoud.2.sharifianmazraehmollaei@aalto.fi; konstantin.simovski@aalto.fi).

Ali Sharifian Mazraeh Mollaei is with the School of Electrical Engineering, University of Tehran, Tehran 1417935840, Iran (e-mail: a.sharifian@ut.ac.ir).

Color versions of one or more figures in this article are available at https://doi.org/10.1109/TAP.2021.3111347.

Digital Object Identifier 10.1109/TAP.2021.3111347

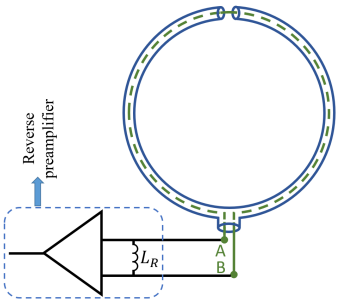

Fig. 1. Schematics view of the initial HIC introduced in the previous work [11].

in our case, the simple mutual overlapping of conventional loops is not very helpful.

Lately, a new type of loop antenna for UHF MRI applications named high-impedance coil (HIC) has been introduced and studied in works [11], [12]. This loop antenna is made of a coaxial cable with a gap in the loop shield at the point opposite to the antenna port, whereas this port is connected to the cable central conductor through a tiny hole in the shield. This kind of loop experiences the parallel-circuit resonance at its first eigenmode. The idea of the first HIC in work [11] was to simply decrease the current in the receiving antenna and consequently to reduce its scattering, which mixes up to the signal and brings noises. In this work, a reverse preamplifier and an inductor shunted with this preamplifier, as shown in Fig. 1, play a key role in the antenna operation. In fact, for conventional receiving coils, their connection to usual preamplifiers with very high input impedance is a common way to decouple them. Then, the impedance seen by the induced EMF is very high, and therefore, the induced current is very small. It implies almost no secondary radiation by coils and grants their decoupling. However, the coil introduced in [11] needs a rather low impedance of the antenna port to perform properly in reception. Therefore, instead of a usual preamplifier, a reverse preamplifier is needed. As we understood from [12], the high self-impedance Z of the HIC not only reduces the scattering but also grants the self-decoupling to an array because the mutual impedances of the reference HIC with the other HICs of the array turn out to be small compared to Z. However, it was so only in the receiving regime. At the first glance, it seems that, in the reciprocal system, the same ratio of the self-impedance and mutual impedance should hold in the transmitting regime. However, a detailed analysis showed that it was not so [13].

In the receiving regime, the EMF is induced on the cable exterior. Since the shunting capacitance of the gap is very small, the voltage induced in the gap splits onto two halves applied in parallel to two cable lines—halves of the cable loop connected to the antenna port. Therefore, the impedance of the parallel connection of two cable lines with the common load—antenna port—has the physical meaning of the impedance loading the induced EMF [13]. This impedance at the operational frequency experiences parallel resonance. At this resonance, the current induced on the cable loop exterior turns out to be very low, and the name of HIC is fully justified. In the transmitting regime, the HIC operates in a different way because the resonant mutual impedance between two HICs is not much smaller than the self-impedance of each one (in accordance to [13], mutual impedance also experiences a parallel resonance). Therefore, in the transmitting regime, the HIC introduced in [11] has nearly the same self-decoupling potential as conventional loop antennas.

In [12], the authors claimed that the same antenna as [11] operates as a HIC also in the transmitting regime if one connects it to another matching circuit and changes the operational frequency. However, in this case, the transmitting HIC is detuned from the parallel resonance. It was tuned in [12] by a matching circuit composed of three capacitors, whereas the input resistance beyond the resonance of the coil was not high enough and turns out to be comparable to the losses. The decoupling in [12] was achieved by the price of a certain reduction of the antenna efficiency in the transmitting regime. It does not imply the damage for the imaging since there is room for the signal power increase. However, if we target also the radiation efficiency, there is room for further improvement of the technical solution [12]. This was done in our work [13]. In this article, the HIC was modified so that to satisfy the governing concept of high self-impedance of each coil compared to its mutual impedances in both transmitting and receiving regimes. It was achieved without the damage for the radiation efficiency closely related to the transmitting efficiency. Our modification was the introduction of additional symmetrically located gaps to both the shield and inner wire of the cable. Our design solution was practically targeted to the scanning of a human head with an array of eight HICs. This application allowed us to design the diameter of the antennas close to $\lambda/2\pi$ (lambda is operating wavelength), i.e., 16 cm.

In works [14]–[16], the authors used multiturn loops of similar sizes and several symmetric gaps so that to shift the resonance frequency of the fundamental mode of the coils. Even though the achieved results in these works show enhancement of radiation efficiency and SNR, the coupling between the adjacent and nonadjacent loops in the transmitting regime was not studied in these works. In work [17], the authors studied the patient comfort and decoupling of the HIC introduced in [11] in a triangular array. Yet, the acceptable coupling coefficients on the level lower than -8 dB were achieved in works [11], [12], [17] only because the arrayed HICs were heavily loaded by the body phantom. It is a highly refractive and very lossy object, and most of the antenna accepted power is transferred to the phantom. In this situation, the field transmitted to the other array elements is much lower than that in the case of an arrayed coil located in free space. Meanwhile, in [13], we achieved the same (even better) decoupling level in free space.

In this article, we report a qualitative development of the research started in our work [13]. We suggest a novel HIC, which grants a new functionality to an arrayed UHF MRI radio frequency coil. Now, the array elements of magnetic-dipole type operate in two very different frequency bands. In both these bands, they are strictly resonant and are well decoupled in both transmitting and receiving regimes.

II. Our Technical Ideas

A. Problem Formulation

The decoupling of HICs in both receiving and transmitting regimes has been already achieved in [13] for a single band. We aim to engineer the resonance bands of our coil so that the antenna array could scan the hydrogen and phosphor isotopes in a 7 T MRI machine: the low-frequency resonance band is centered at 121 MHz and the high-frequency one at 298 MHz. In practice, we need eight coils around the organ at a sufficiently small distance from it because the near-field coupling to the inspected body part is necessary for a proper transceiver regime [1], [2]. Therefore, we choose the same size of our new coil as that in [13] with a diameter of 16 cm. If we make it larger, it will not be suitable for scanning the head and, moreover, feet or knees. If we make it smaller, the coil diameter will be much smaller than $\lambda/2\pi$ at the first frequency and then will imply the radiation resistance lower than 1 Ω. Making the dissipation loss in the antenna much lower than 1 Ω is not a realistic task, and such an antenna will be very inefficient. The diameter of 16 cm is a good compromise for both transmitting and receiving regimes. However, for the given size of the radiator, the radiated power is proportional to the fourth power of the frequency, meaning that, at the second frequency, the antenna radiation is higher than that at the first frequency by order of magnitudes. Therefore, it is not enough to suppress the mutual coupling for adjacent array elements at this band, and nonadjacent elements also need to be decoupled. This problem has been already targeted in works [6], [8], [9]. However, in these works, it was formulated and solved for a single operational band. For us, the formulation is challenging because the approaches for self-decoupling should be different for two frequencies. Though the governing idea of the whole approach is still that of the HIC, it is now a dual-band transceiver high-impedance coil (dual-band TRHIC) and must be designed in a different way.

The problem can be formulated as a set of questions to be answered.

1) How to tune the resonance frequency of a coaxial cable loop antenna in a very wide interval of possible frequencies?
2) How to make such an antenna dual-band with very different resonant frequencies?
3) How our arrayed antennas do operate in the low-frequency band in the transmission regime?
4) How do they operate in the high-frequency band in the transmission regime?
5) How do they operate in the receiving regime in both bands?

A possible answer to these questions is given by a cable loop loaded by two gaps in the shield located asymmetrically. No gaps in the inner wire (except the antenna port connection) are needed. Varying the positions of two gaps in the shield, we may shift the resonance frequencies of the loop eigenmodes tuning the antenna to resonances at very different frequencies. Moreover, with two gaps we may engineer the properties of the resonant modes that grant the needed self-decoupling.

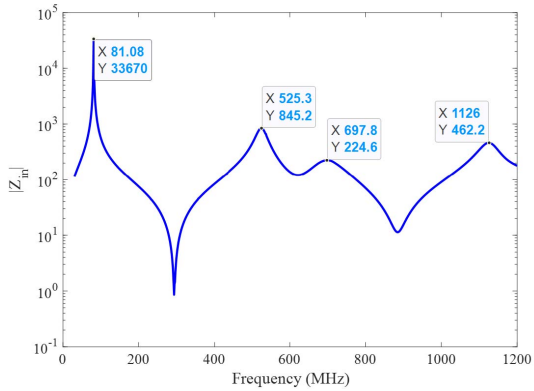

Fig. 2. Absolute value of the input impedance of the initial HIC with the design parameters from [13] in the transmitting regime. Frequencies at which the name HIC is justified are marked.

B. Modes

Before discussing our method, we need to explain the issue of eigenmodes in a HIC starting from its initial design. Fig. 1 depicts the initial HIC introduced in [11] and [12]. In [13], we showed that the equivalent circuits of this coil are different in the transmitting and receiving regimes. Moreover, the frequencies of the eigenmodes in the transmitting and receiving regimes are different. According to the circuit model of [13], in the transmitting regime, two transmission lines of coaxial cable are connected with one another through the inductive impedance corresponding to the outer surface of the shield. In the receiving regime, the same cable lines are excited by the voltage applied to the gap (see above) and loaded by the impedance connected to the antenna port. As it is shown in Fig. 1, it is the inductive impedance $j\omega L_R$ weakly shunted by the rather high impedance of the operational preamplifier—reverse preamplifier.

Using the commercial software CST Microwave Studio, we simulated the performance of the initial HIC (see Fig. 1) in a wide range of frequencies in the transmission. Here, the parameters of the HIC are the same as those used in [13] (except the added gaps to the inner wire and the shield at the feeding point). Fig. 2 shows the magnitude of the antenna input impedance. We see that, in the frequency range 30–1200 MHz, there are four frequencies at which the input impedance of the HIC experiences parallel resonance. These resonances are marked in the plot. Around 300 and 900 MHz, the antenna experiences the series resonances. At these resonant frequencies, the performance of the cable loop antenna is qualitatively the same as that of a conventional coil, and the name HIC is not justified (the fundamental mode of a conventional coil is a series-resonant one, and the simulated HIC experiences series resonances at these frequencies).

We have done the same calculations for the receiving regime. In this regime, all resonance frequencies of the antenna are slightly different. However, these differences are small in our simulations because the inductive load created by the effective receiving loop (exterior of the shield) turned out to be the value of the same order as ωL_R—the inductive shunt of the signal source in the transmitting regime. In Fig. 3, we plot the current distribution over the shield exterior at four

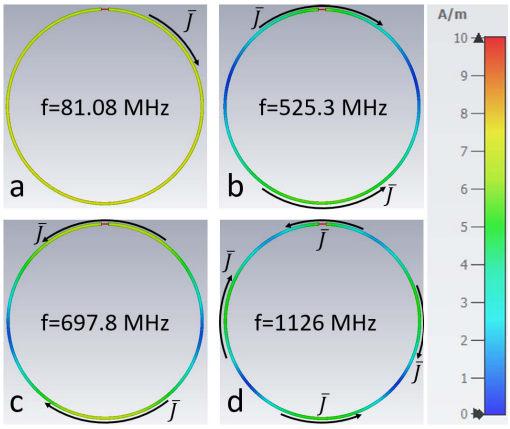

Fig. 3. Current density distributions over the shield exterior of the basic transmitting HIC at four resonance frequencies marked in Fig. 2. The black arrows in each panel show the direction of current density. These distributions allow us to judge the multipole content of the loop current. (a) f = 81.08 MHz. (b) f = 525.3 MHz. (c) f = 697.8 MHz. (d) f = 1126 MHz.

parallel resonances marked in Fig. 2. This figure shows that the first resonance (81.08 MHz) corresponds to the magnetic dipole mode of the loop current. The series resonance at 300 MHz corresponds to the hybrid mode when both magnetic and electric dipole moments are present in the loop. Second (525.3 MHz) and third (697.8 MHz) parallel resonances correspond to the electric dipole mode. Fourth (1126 MHz) parallel resonance is that of the magnetic quadrupole. Our purpose is to shift the first resonance to 121 MHz, to shift the second resonance to 300 MHz, and to engineer this hybrid mode so that the electric and magnetic dipoles are balanced in it. If they are balanced, the fields of the electric and magnetic dipoles sum up at one side of the loop, and at the opposite side of the loop, these fields cancel out. It means that the loop located at this side will be decoupled with the reference loop. In [13], by adding symmetric gaps in the shield and inner wire, we engineered a blue shift of the magnetic dipole mode and the red shift of the electric dipole mode. This way, we overlapped two resonances and created a hybrid mode with the eigenfrequency 300 MHz where the magnetic and electric dipoles were balanced.

III. Methods of the Study

A. Theory

To better explain the operation of our dual-band TRHIC, we have to remind how the initial HIC introduced in [13] operates. According to [11]–[13], decoupling in the receiving regime means that the induced current in a receiving HIC is very low. This results in a very low scattered electromagnetic field created by a receiving coil at the neighboring ones. Recall that the initial idea of the HIC was to design the loop antenna so that the resonant impedance to which the induced EMF is connected is high enough (of the order of 1000 Ω) compared to that of the conventional coil. The current smallness implies the domination of the self-impedance over the mutual impedance between two adjacent coils. From the technical point of view, the relatively high value of the self-impedance connected to

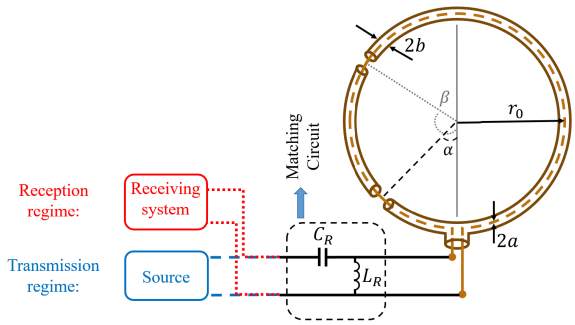

Fig. 4. Schematics of the TRHIC. In the transmitting regime, the source is connected to the structure through the matching circuit. In the receiving regime, the same matching circuit connects the TRHIC to the receiver.

the EMF is achieved due to the impedance inversion in a quarter-wave transmission line. Two halves of the cable loop connected to the gap operate as pieces of the transmission line and transform a low impedance of the receiving circuit (if we look at Fig. 1, we see that this impedance is of the order of $j\omega L_R$) into a high impedance loading the EMF. Though the induced current on the shield exterior is very low, the induced EMF captured by two transmission lines and delivered to the receiver is substantial. This is how the initial HIC operates in the receiving regime at the magnetic mode resonance.

In [13], we blue-shifted the frequency band by adding a bottom gap to the shield and red shifted the electric mode resonance by adding two symmetric gaps to the inner wire. In this way, we tuned the hybrid mode to the required frequency. However, due to these symmetrically added gaps, all eigenfrequencies shifted over the frequency axis, and it was not possible to independently tune the resonance frequency of different modes. In this article, we do not split the inner wire and achieve the claimed goal by introducing two asymmetrically located gaps to the shield, which allows us to tune the eigenfrequencies of two dipole modes independently.

Fig. 4 shows our proposed antenna. To start designing, a single asymmetrically located gap, located in our example at the angle $\alpha = 20°$, makes the cable loop antenna unbalanced—the left part of the coaxial cable is much shorter than the right one. In this case, the shorter transmission line connecting the EMF to the matching circuit in the counterclockwise direction is responsible for the low-frequency parallel resonance frequency (121 MHz). On the other hand, the longer cable line is responsible for the high-frequency parallel resonance (about 220 MHz). This counterintuitive result has a simple qualitative explanation. A piece of a cable of length l between the gap and the antenna port connects the inductive impedance $j\omega L_{\text{shield}}$ of the external loop to the antenna port. Another piece of a cable of length $2\pi r_0 - l$ (r_0 is the loop radius) connects this impedance to the same antenna port in parallel. Since the lengths l and $2\pi r_0 - l$ are very different, the antenna port sees two sets of parallel-circuit resonances. At the resonance corresponding to one of two cable lines, the presence of the second one is not important. One parallel resonance in the antenna port holds due to the short line when the resonance condition $l + \delta l = (2m + 1)\lambda/4$ is fulfilled, where $m = 0, 1, 2, \ldots$, and δl is an elongation of the cable line equivalent

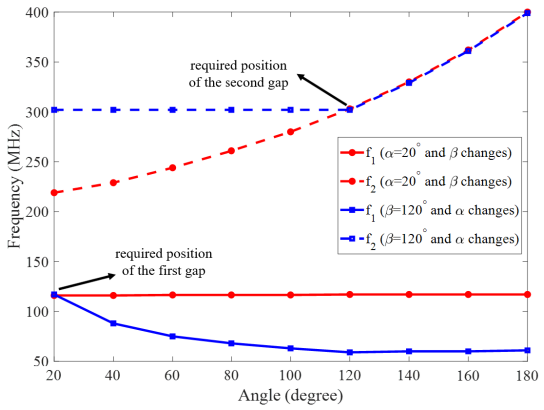

Fig. 5. Resonance frequencies of the first and second modes: while $\alpha = 20°$ and β changes between 20° to 180° (we see that the first resonance occurs at the same frequency, while second resonance shifts to higher frequencies), and $\beta = 120°$ and α changes between 20° to 180° (when $\beta > \alpha$, we see that the first resonance shifts to lower frequencies, and the second resonance occurs at the same frequency—298 MHz. When $\beta < \alpha$, we see that the first resonance occurs at the same frequency—60 MHz—and the second resonance shifts to higher frequencies).

to the inductive load $j\omega L_{\text{shield}}$. Thus, the short part of the broken loop in the frequency region of our interest is shorter than quarter-wavelength, meaning that $m = 0$. In the same frequency region, the longer part exceeds quarter-wavelength but is shorter than half-wavelength, and for it, the parallel resonance condition holds with $m = 1$. In other words, the short cable line offers the resonance at a wavelength

$$\lambda_1 = 4(l + \Delta l) \tag{1}$$

and the long cable line at

$$\lambda_2 = 4(2\pi r_0 - l + \Delta l)/3 \tag{2}$$

where definitely $\lambda_1 > \lambda_2$.

To see how the location of our single asymmetric gap affects these two resonant wavelengths (frequencies), we simulated a HIC with one gap in the shield varying α from initial 20° to final 160°. In these simulations, the design parameters of the HIC except the gaps were kept the same as in [13]. We retrieved the frequencies of two resonances connecting a lumped power source to the antenna port in our simulations. When α increases, the length of the shorter cable line increases resulting in the red shift of the lower resonance. At the same time, the length of the long line decreases, resulting in the blue shift of the second resonance. Thus, we obtain two parallel resonances with one gap. However, with one gap, we cannot engineer the needed operational frequencies of the coil.

Now, it is time to add the second gap, which offers us the needed degree of freedom. Based on our simulations, the first gap at $\alpha = 20°$ offers the resonance at the Phosphor frequency (121 MHz) not perturbed by the second gap. The second gap at $\beta = 120°$ offers the resonance at the hydrogen frequency (298 MHz) not perturbed by the first gap. To analyze the effect of the second gap over the coil performance, we simulated the case when the first gap $\alpha = 20°$ is fixed and the second gap β changes between 20° to 180°. Then, we fixed the position of the second gap at $\beta = 120°$ and changed the position of the first gap. Fig. 5 shows the simulation result. As expected, when $\alpha = 20°$ and we change β from 20° to 180°, we shorten the length of the right transmission line, resulting in the blue shift of the second resonance (red dashed line in the figure), while the length of the left transmission line from the feeding point to α remains the same, resulting in the constant resonance frequency of the first mode (red solid line). When $\beta = 120°$ and we change α from 20° to 180°, in the case that $\beta > \alpha$, then the length of the left transmission line increases, the resonance frequency of the first mode decreases (blue solid line), and the length of the right transmission line remains the same, leading to the same resonance frequency (blue dashed line); in the case that $\beta < \alpha$, then the length of the left transmission line remains the same and no frequency shift for f_1 (the blue solid line between 120°–180°), and the length of the right transmission line decreases resulting in a blue shift of f_2 (blue dashed line between 120°–180°). The decoupling functionality in the transmitting regime would be compromised by such **a** location of the gaps. Our target is dual-band transceiver HIC–TRHIC, and we have to locate the gaps so that the performance of the coil is nearly optimal in both receiving and transmitting regimes. The optimal performance in reception occurs when the impedance loading the induced EMF is maximal. Here, the EMF is split onto two voltages applied to two gaps, and the impedance of the circuit connected to the antenna port (nearly equal to $j\omega L_R$) is transferred to these gaps being transformed by the two cable lines. This transformation ensures the high absolute value of the impedance seen by the EMF. The optimal performance of the HIC in the transmitting regime occurs when the antenna is self-tuned to the operation frequency [13]. In accordance with [13], the frequencies of the optimal reception and optimal transmission are slightly different. As to the gap in our TRHIC, we optimize its location for the transmission regime and check that the impedance seen by the induced EMF is high enough for the proper operation of the antenna in reception (not ideal but acceptable decoupling in reception). This deal between the reception and transmission delivers the optimal angles $\alpha = 20°$ and $\beta = 120°$, as shown in Fig. 4. The impedance seen by the induced EMF at the frequency 300 MHz is of the order of 1000 Ω, i.e., is not as high as that of the HIC from [13]. However, conceptually, it is still HIC also in the receiving regime since the mutual impedance at the resonance in the receiving regime turns out to be much smaller.

Unfortunately, it is not possible to build a model that would allow us to find the required locations of our asymmetric gaps analytically because two gaps located beyond the points $\alpha = 20°$ and $\beta = 120°$ interact with one another, and the impedances at these points cannot be easily found. Here, it is difficult to suggest a general equivalent circuit, and it is reasonable to optimize the gap positions using a full-wave electromagnetic solver.

Now, let us briefly discuss the decoupling issue. Transmission coefficients between two coils denoted as S_{12} and S_{21} expressing their mutual coupling can be calculated as follows:

$$S_{12(21)} = \frac{2Z_0 Z_{12(21)}}{(Z_{11} + Z_0)(Z_{22} + Z_0) - -Z_{12}Z_{21}} \tag{3}$$

where Z_0 is characteristic impedance of the transmission line connecting the antenna external circuit to the antenna, and Z_{11}, Z_{22}, Z_{12}, and Z_{21} are, respectively, self-impedance of antenna 1, self-impedance of antenna 2, and mutual impedance seen by antenna 1 and antenna 2, respectively. Due to the reciprocity $Z_{12} = Z_{21} \equiv Z_m$, $S_{12} = S_{21} \equiv S_m$. In our case, antennas 1 and 2 are the same, i.e., $Z_{11} = Z_{22} \equiv Z$.

Evidently, if $\gamma = |Z_m/Z| \ll 1$, we have $|S_m| \ll 1$, and two antennas are almost decoupled. Achieving $|Z_m/Z| \ll 1$ is possible in two ways. The first way is the increase of Z for a given Z_m. This is the concept of the HIC from [11]. The second way is to decrease Z_m for a given Z.

To achieve the decoupling of our TRHICs in the receiving regime in both frequency bands, we use the first strategy: increase of Z for a given Z_m. In the receiving regime, the coupling is that between the exteriors of coils 1 and 2. The echo signal induces the currents on the exterior of the cable loops, and the coils are coupled via these currents. These currents are small because the self-impedance loading of the EMF is high. The additional EMFs induced in the coils on each other are proportional to these small currents and are also small. The mutual impedance at the resonance cannot exceed the radiation resistance, which is in the order of 1 and 20 Ω at 120 and 300 MHz, respectively. Thus, in the receiving regime, $|Z_m|$ is lower than the self-impedance by orders of magnitude and in works [11]–[13].

However, in the transmitting regime when the value of input impedance seen by the antenna port is high, it is not the guarantee of the HIC operation because the mutual impedance $|Z_m|$ can be of the same order (the mutual impedance is also transferred to the antenna port through the same transmission lines). In our case, if two TRHICs are located aside with a gap of the order $d \sim \lambda/30$ (the same configuration applied in [13]), the factor γ is high. It does not allow us to achieve the resonant coupling coefficient S_{12} below -8 dB at both frequencies. This level of coupling is demanded in the presence of the inspected body, whereas, in this work, we consider the array in free space. Therefore, we hope that our coils are suitable for dual-band operation with reduced coupling in the transmitting regime even if the array is a chain of loops located with a small gap between them without mutual rotations of the adjacent loops. This design is needed for scanning closely located small organs. For example, scanning the fingers implies one coil per finger. In this case, all coils are fed from one side, and their overlapping is not allowed [11].

Another practical design of the array allows us to achieve the needed decoupling of the transmitting coils even located in free space at both frequencies. For that, the coils are mutually overlapped. The coupling of the array elements is sufficiently small in the band of 300 MHz for the coils located aside even without the use of the advantage granted by the balanced hybrid mode. If we overlap the coils so that to cancel the mutual inductance, the coupling drastically decreases at the first one where the coupling is quasi-static.

The third practical design of our array implies the 180° mutual rotation of the adjacent coils, i.e., their gaps are located upside-down. As to the antenna ports, they can be located either at the opposite sides of the chain (the same arrangement as in [13]) or on the chain axis in the alternating arrangement. Both these arrangements enable the reduction of the mutual coupling in the array granted by the balanced hybrid mode in the second operational band. Moreover, in this array, the adjacent coils are mutually overlapping. Overlapping grants the decoupling at the first frequency without increased coupling at the second one. In this design, we implement the concept of transmitting HIC reducing the mutual impedance in both bands.

Since this article is only a step toward a practical design of the dual-band arrayed TRHIC for UHF MRI, we simulate and measure as follows.

1) A Single TRHIC in free space.
2) An array of two TRHICs with and without overlapping, antenna ports has located on either side of the array or upside-down.
3) An array of three TRHICs without overlapping, antenna ports is located aside from the array.

The results of these studies are sufficient in order to confirm the claimed advantages of our TRHICs and start the next stage of our research toward the practical array of dual-band TRHICs.

B. Numerical Simulations

Full-wave simulations have been carried out by CST Microwave Studio, Frequency Domain. These simulations allowed us to numerically analyze the following features.

1) Resonance frequency of different modes excited in the TRHIC (we see that we really can engineer these frequencies).
2) Distribution of the field at these frequencies in the transmitting regime: balanced hybrid mode at the needed frequency is achievable.
3) Self-impedance (Z) and mutual (Z_m) impedance of two TRHICs in the transmitting regime: small $\gamma = |Z_m/Z|$ is obtained.
4) Comparison of the factor $\gamma = |Z_m/Z|$ with that calculated for the known HIC from our previous work [13]: TRHICs grant better decoupling in the transmitting regime than the best of known HICs in the case that coils are not overlapped.
5) Current induced on the exterior of the shield in reception: the current is low enough to grant the decoupling in reception.
6) Coupling of TRHICs in a linear array: the array is decoupled in both regimes.

For simulations in the transmitting regime, we connect a lumped power source with 50 Ω output impedance to the TRHIC. In this way, we retrieve the resonance frequency of different modes and calculate the radiated fields in the mismatched regime. Using these results, we could see where to locate the gaps for obtaining the dual-band regime with the needed mode properties. After designing the dual-band TRHIC with the balanced hybrid current mode at the second operational frequency, we simulate two TRHICs either located

next to each other or overlapped and calculate the Z-matrix of the array. By comparing these Z-matrices with that of the known HIC in [13], we can see that our TRHIC is advantageous in the hydrogen-frequency band compared to the known single-band HIC. Calculating the current distribution in the transmitting TRHIC and the magnetic field around it, we see that this advantage really results from the interference of the electric and magnetic components of the hybrid mode. As to the first resonance frequency, we obtain the huge absolute values of the self-impedance and noticeably lower values for the mutual impedances of two overlapping TRHICs.

To check the prerequisite of decoupling in reception, we excite the TRHIC by a plane wave. The plane wave is polarized so that its magnetic field is orthogonal to the surface of the coil and induces the EMF on the cable shield. In this case, the matching circuit is the same as in the transmission regime and includes L_R shunting the port of the coil. Similar to [13], we numerically find that the induced current on the shield is very low—much lower than that induced in a conventional loop of the same diameter $2r_0$. It means that the field scattered by a receiving TRHIC at the centers of the adjacent TRHICs must be very low and the decoupling in the receiving regime must be achieved.

Finally, we simulate the S-parameters of an array made of three TRHICs at the second resonance frequency. Due to the high impedance seen at the ports of these TRHICs and 50 Ω sources, there is a huge mismatch between sources and coils, which results in the reflection of most of the power to the sources. In this case, using the matching toolbox of the software, we add optimal lossless matching circuits between the sources and the TRHICs. The matching circuit consists of a parallel inductor L_R and a series capacitor C_R, as shown in Fig. 4. By calculating $S_{12} = S_{21}$, $S_{13} = S_{31}$, and $S_{23} = S_{32}$ in this matched case, we can see the coupling between our TRHICs in the array of three elements.

In all these simulations, the inner wire and shield of the coaxial cable are made of copper, the relative permittivity of the coaxial cable substrate is $\epsilon_r = 2.2$, and other parameters of the TRHIC are given as follows $r_0 = 80$ mm, $b = 1.3$ mm, and $a = 0.5$ mm. The thickness of the shield is equal to 0.1 mm, and the length of the gaps is 3 mm. For matching two TRHICs at the first resonance frequency, two of the same matching circuits constituted of a parallel inductor $L_R = 620$ nH and a series capacitor $C_R = 0.28$ pF are connected between the sources and the coils. Note that the matching circuit for the first resonance is different from that we need to match the TRHIC to the transmitter or receiver at the second resonance. For matching three TRHICs at the second resonance frequency, two matching circuits have $L_R = 250$ nH and $C_R = 1.7$ pF (for TRHICs located at the array ends), and a matching circuit with $L_R = 270$ nH and $C_R = 1.75$ pF is connected to the central TRHIC. The main goal of these simulations was to study the coupling at the second operation frequency for the parallel and upside-down geometries of the antenna ports. The distance between the edges of adjacent TRHICs in this study has varied in the interval d = 1–3 cm.

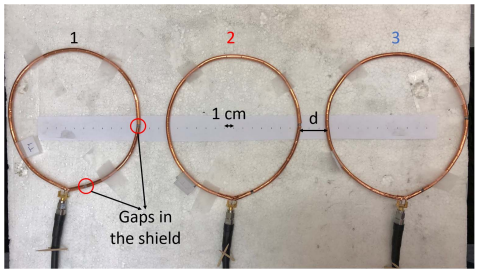

Fig. 6. Fabricated TRHICs located in a linear array with the 30 mm distance from each other.

C. Experiment

To confirm our theory and numerical simulations, we built three proposed TRHICs. In our experiment, we aimed to: 1) measure the input impedance of our proposed TRHIC representing resonance frequencies of two different modes; 2) measure the Z matrix of two TRHICs located next to each other (distance between them is 3 mm) at the second frequency; 3) measure the S-parameters of two overlapped TRHICs at the first and second frequency; and 4) measure the S-parameters of three TRHICs located next to each other (at the second frequency). For fabrication, we used the inner wire and substrate of the coaxial cable Bedea 1085 RG 59 ($a = 0.2875$ mm and $\epsilon_r = 2.2$) and used copper tape to make the shield. Using the copper tape, we could easily change the position of the gaps and tune the resonance frequencies. Using Keysight PNA Network Analyzer N5225A, we measured the S-parameters of the array. In order to understand how the coupling at the second frequency depends on the distance, we changed the distance between the TRHICs from $d = 10$ mm to $d = 30$ mm and measured the resonant S-parameters.

To avoid the difficult fabrication of tunable matching circuits, we used virtual matching circuitry from the schematic toolbox of AWR software. In this virtual toolbox, first, two of the same matching circuits with $L_R = 520$ nH and $C_R = 3.9$ pF were connected to the TRHICs to match the coils to 50 Ω at the first resonance frequency. To match them at the second resonance frequency, two of the same matching circuits with $L_R = 90$ nH and $C_R = 3.7$ pF were connected to the edge TRHICs, and a matching circuit with $L_R = 105$ nH and $C_R = 2.5$ pF was connected to the middle TRHIC.

IV. Main Results

A. Single TRHIC

First, we simulated our coil in the transmission regime. In accordance with Fig. 5, we locate two asymmetric gaps initially at the points $\alpha = 20°$ and $\beta = 120°$ and then vary these angles. The simulations confirmed that the optimal positions of these gaps were the initial ones. Next, we fabricated three samples of a TRHIC and measured the self-impedances of the samples. Fig. 6 shows three fabricated TRHICs, and the location of the gaps is marked by red circles.

Self-impedance of the simulated and measured TRHICs located in free space is shown in Fig. 7(a). Though the resonant values of the measured impedance real and imaginary

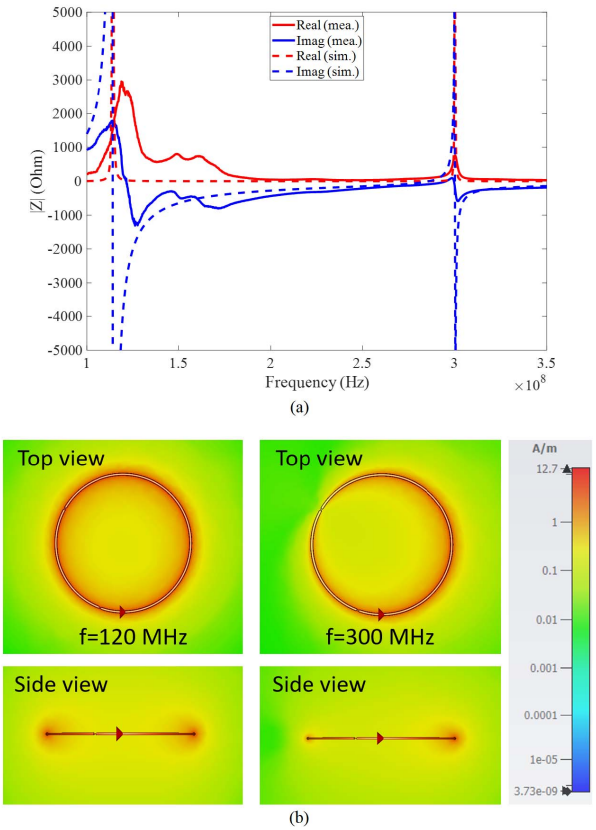

Fig. 7. (a) Simulated and measured self-impedances of our TRHIC versus frequency in free space. (b) Color maps of the normal component of the magnetic fields produced by our TRHIC at two resonance frequencies (simulation).

parts turned out to be twice smaller than the simulated ones, it is not a failure of the model. This reduction of amplitude resulted from losses in the copper tape and the effect of the nonideal surrounding medium. Our purpose was to predict that two resonance frequency bands are achieved, and they are tuned correctly. Note that, by changing the ratio between the diameter of the inner to the diameter of the shield, changing the relative permittivity of the cable [11], and changing the position of the gaps [13], it is possible to make TRIHCs with different sizes resonating at the same frequencies or the TRHIC of same size resonating at different frequencies.

As it was noted above, the mutual impedance near 300 MHz is comparable with the self-impedance. For reducing the mutual impedance, we can possibly use the destructive interference of the magnetic and electric dipole fields like we did in [13]. In Fig. 7(b), we plot the simulation results of the radiated magnetic field at the frequencies of two resonance bands. At the first resonance frequency, this field distribution nearly coincides with the static magnetic field of a uniform circular current that can be calculated analytically. It means that the coupling in the array can be reduced by overlapping the adjacent coils.

B. Two TRHICs

To decouple two neighboring TRHICs in the transmission regime at the first operational band, we overlapped them. The mutual inductance is canceled when the intersection area is 15% of the loop area. However, decoupling at the first frequency is a rather easy task. A more interesting task is to decouple the TRHICs at the second frequency using the effect of the balanced mode.

Inspecting the right panel in Fig. 7(b), we see that the near magnetic field nullifies not at the azimuthal angle $\phi = 180°$ as it was in [13] but at the angle $\phi = \beta = 120°$. The reason is the tilt of the effective electric dipole of the loop current—the direction of the electric dipole is determined by the gap responsible for its resonant excitation at 300 MHz. Therefore, to obtain the best possible decoupling in the second band, two TRHICs must be located back to back from the gap point at $\beta = 120°$. We measured the coupling between two TRHICs arranged when the coils are located back to back with the distance $d = 1$ mm between their edges and found that, even in the matched regime when $S_{11} = S_{22} = -30$ dB, the resonant coupling level is amazingly low (S_{21} is -42 dB at 298 MHz).

However, this arrangement is optimal only for an array of two TRHICs. If the third element is added, it will be highly coupled to the middle TRHIC because the area of the high magnetic field created by the middle coil is exactly opposite to the area where its field is nearly zero. In order to optimally decouple our TRHICs, the antenna ports of the coils forming a linear chain should be located, as shown in Fig. 8(a). In this case, the areas of high near magnetic field created by any coil minimally intersect with the other ones. This geometry of the practical array is compatible with the overlapping of the adjacent loop (needed to decouple them at the first frequency) and, of course, keeps the self-decoupling in the receiving regime.

However, the alternating tilts of the antenna ports may be difficult to implement in practice. The arrangement with the collinear location of the ports shown in Fig. 8(b) also promises the reduction of the coupling. In this arrangement, the area of the high magnetic field created by any coil rather weakly intersects with the adjacent coil. To clarify, because the direction of the electric mode is rotated with respect to the antenna port, we may decompose the electric mode into two electric modes: one in the x-direction and one in the y-direction. In [13], electric modes are aligned in the x-direction, which results in low electric coupling between two coils. For the arrangement shown in Fig. 8(b), electric coupling between decomposed electric modes in the y-direction is rather high. Therefore, the electric coupling coefficient is high enough to compensate magnetic coupling coefficient even if the coils are not overlapped. This is the reason why coupling is lower between coils arranged in this way compared to that of the coil differently arranged in [13] [as shown in Fig. 8(c)]. We calculated and measured the coupling between two TRHIC whose antenna ports are located namely in this way [see Fig. 8(a)]. In order to achieve the decoupling also at the first frequency, we used the overlapping. The optimal overlapping at the first frequency is 15%, whereas, at the second frequency, the optimal overlapping is 20%. To minimize the mean mutual coupling of two coils arranged at both frequencies, we overlapped them by 17% and 18%. In Fig. 9(b), we plot the measured self-impedance and mutual impedance of these

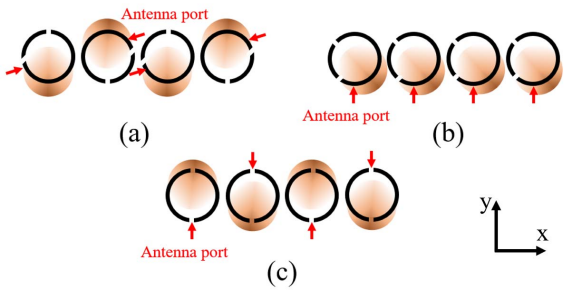

Fig. 8. (a) Chain of transmitting coils with optimal locations of the antenna ports. Sketched field spots (areas of the high magnetic field created every coil) practically do not intersect with the neighboring coils. By overlapping, one can obtain the complete decoupled situation between neighboring coils. (b) Chain with suitable locations of the antenna ports (especially for scanning fingers). (c) Chain with suitable locations of the antenna ports based on the HICs presented in [13].

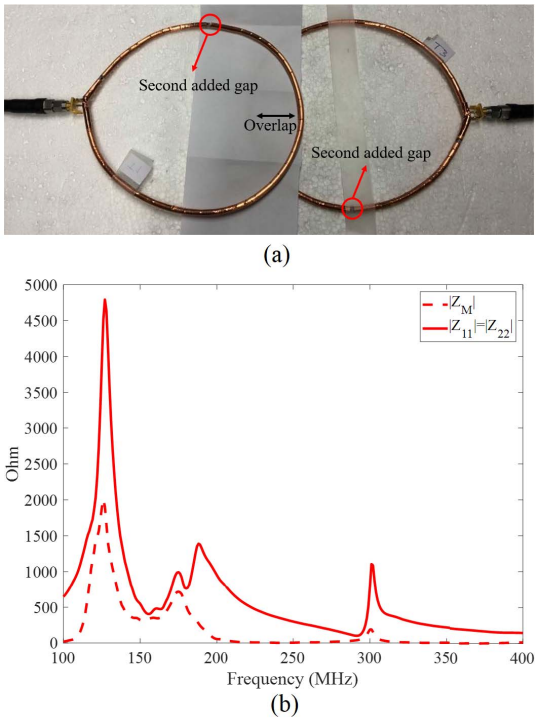

Fig. 9. (a) Two TRHICs arranged as in Fig. 8(a) and overlapped optimally. (b) Comparison of the self-impedance Z and mutual Z_m impedance of two TRHICs in this case.

coils. Judging upon (3), when $\gamma = |Z_m/Z| \ll 1$, the coils must be decoupled. In this figure, we see that, at both operational bands, the ratio γ is really small (0.36 at the first frequency and 0.21 at the second one). Of course, the input impedance of both coils at the first frequency and that at the second frequency are different, and the matching circuits for the two bands should be different as well. When the virtual matching circuits described above are used, we have at 121 MHz $S_{11} = S_{22} = -30$ dB and $S_{21} = S_{12} = -10.5$ dB and at 298 MHz $S_{11} = S_{22} = -30$ dB and $S_{21} = S_{12} = -16.6$ dB. Also, we have measured the mutual coupling between two TRHICs overlapped optimally for decoupling at the second band (20% overlap). In this case at 298 MHz, we have $S_{11} = S_{22} = -40$ dB and $S_{21} = S_{12} = -23$ dB.

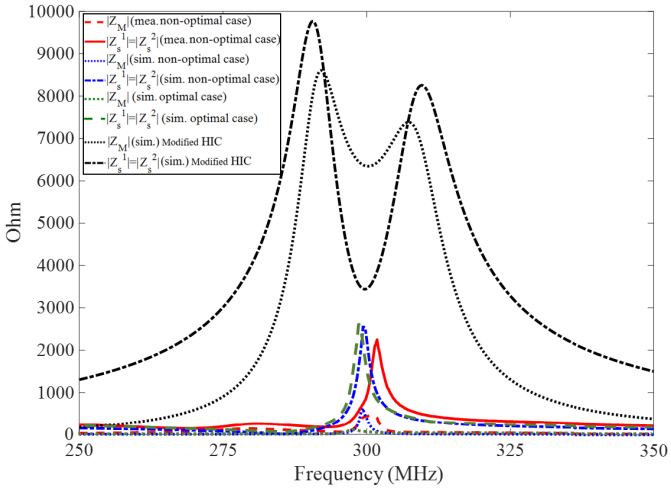

Fig. 10. Comparison of the self-impedance Z and mutual Z_m impedance of two proposed TRHICs with those of two HICs from [13] in the band covering 300 MHz. To obtain these results, in the first case, two TRHICs are located aside each other without any rotation—nonoptimal case; in the second case, two TRHICs are located back to back from the second added gap point of view—optimally located [as shown in Fig. 9(a)]. In the third case, two HICs from [13] located next to each other upside down [as shown in Fig. 8(c)]. The sizes of all coils are equivalent, and the distance between coils is $d = 3$ cm. Coupling factor $\gamma = |Z_m/Z|$ for two TRHICs positioned optimally, nonoptimally, and for two HICs reported in [13] is nearly equal to 0.09, 0.25 (0.3 in measurement), and 2, respectively.

We see that our theoretical expectations were fully confirmed by these measurements: the dual-band performance of the TRHICs and their decoupling in both operational bands in the transmitting regime are proved. However, this is done only for an array of overlapped TRHICs arranged with their mutual rotation. Let us now consider the case when two TRHICs are located like in Fig. 6 without rotation with the gap $d = 3$ cm between them. As we have already discussed, in this situation, we cannot achieve the needed decoupling at the first frequency in the absence of the body. In the second band, the coupling is sufficiently suppressed. Though the decoupling is not so efficient as in the above cases of the optimal and nearly optimal arrangements, it is better than we have achieved in [13].

We calculated and measured $|Z|$ and $|Z_m|$ for both optimal [see Fig. 8(a)] and nonoptimal [see Fig. 8(b)] cases and compared these frequency plots with the same parameters taken from [13] (in that work, two HICs were also located with the gap $d = 3$ cm). Fig. 10 depicts the results of this comparison. For HICs from [13] in the operational frequency band of 298–302 MHz, the mean value of $\gamma = |Z_m/Z|$ is nearly equal to 2. For our TRIHCs positioned nonoptimally, this value is close to 0.25 in the simulations and 0.3 in the experiment, and for the optimal case, this value is 0.09 (simulated).

To estimate the coupling of the arrayed TRHICs in the receiving regime, we have calculated the current induced on the exterior of the shield at frequencies from 50 to 320 MHz in the case when two TRHICs ideally matched by a virtual matching circuit are coupled in reception. First, we simulated the current induced on the exterior of the single TRHIC excited by a plane wave. This current was taken as a source in

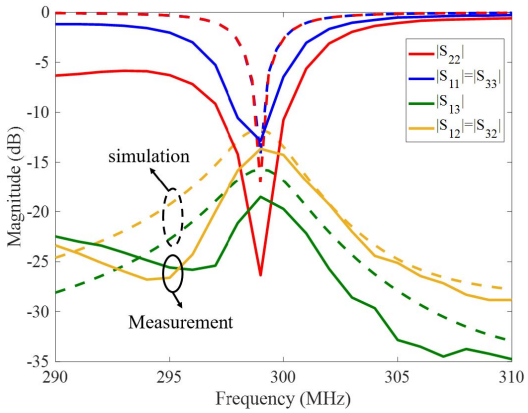

Fig. 11. Experimental and numerical results for the S-parameters of three TRHICs forming a linear array with $d = 3$ cm gaps (matched case). Solid curves are measured; dashed curves of the same colors are simulated.

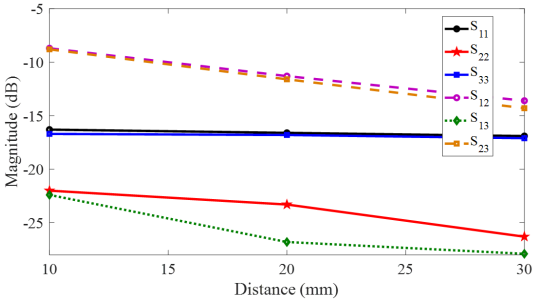

Fig. 12. Experimental results for the S-parameters of three TRHICs forming a linear array with the varying gap between the elements.

our second simulation, where the plane wave was replaced by the second TRHIC (either located aside or overlapped). Of course, in a practical array, the excitation of any receiving TRHIC will be different from both these cases, and in the following, we report the coupling coefficients for both transmitting and receiving regimes. The goal of this simulation was only to check that the induced current is sufficiently small at both 121 and 298 MHz. Really, we have seen that the induced current in two broad bands covering 120 (50–220 MHz) and 300 MHz (250–320 MHz) is smaller than the current induced in a conventional loop (of the same overall size, also ideally matched and similarly excited) by order of magnitude.

C. Three TRHICs

To analyze the coupling between the adjacent and nonadjacent TRHICs in the second band in both transmitting and receiving regimes, we simulated and measured the S-parameters of a linear array of three TRHICs. In both simulation and measurement, we locate three TRHICs without rotation and with the gap $d = 30$ mm in between. In both simulation and measurement, coils were mismatched. It is obvious that these S-parameters refer to both transmitting and receiving regimes of the array since they characterize the reflection coefficients and coupling coefficients of unloaded antennas. Neither matching circuits nor impedances of the transmitter/receiver are involved. After calculating and measuring these mismatched parameters, we have used the virtual matching toolbox of AWR software and matched all these TRHICs to 50 Ω antenna ports.

Fig. 11 shows the experimental results in the matched regime in comparison with the simulations. We see that, at the resonance frequency, $S_{11} = S_{33} \approx -16$, $S_{22} \approx -26$, $S_{12} = S_{21} = S_{23} = S_{32} = -13$ dB, and $S_{13} = S_{31} \approx -28$, which means both adjacent and nonadjacent TRHICs are practically decoupled at the second band.

To understand the impact of the distance between the array elements, we varied d in the range d = 1–3 cm with the step 1 cm and measured the S-parameters again. Since our TRHICs are well decoupled, the change of d does not change the input impedance of each of the three TRHICs noticeably. Therefore, we could use the same virtual matching circuit as the case of $d = 30$ mm. Fig. 12 shows the resonant (298 MHz) S-parameters versus the distance between coils. Based on these results, even for the case when $d = 10$ mm, the coupling between the elements is low (S_{ij} is below -8 dB). This distance theoretically corresponds to higher coupling than that corresponding to the overlapped loops. We did not overlap the elements of this array because, in that case (unlike the case of two coils when both loops are equally overlapped), the input impedance of the central coil will be very different from that of the edge coils, and the results will be not very relevant. Really, in practical coil arrays, there are no edge elements because the array is circular (surrounding the patient's head, leg, and so on). For scanning separate organs, such as fingers, it was enough to study a linear array and to see the decoupling for a positive separation d between its elements.

V. Early Stage of Practical Verification

For preliminary verification of our dual-band TRHICs in practice, we simulate the case when three TRHICs, as shown in Fig. 6, are located above a human body phantom with the same parameters as in our work [13] (permittivity $\epsilon_r = 40$ and conductivity $\sigma = 1.59$ S/m). The presence of the phantom leads to a red shift of resonance frequencies; therefore, we slightly changed the position of the gaps to tune the coils to the proper frequencies. Moreover, most of the radiated signals penetrate the phantom, meaning that the coupling between our coils reduces. Notice that, for each of the bands, a separate matching circuit is needed, and the electronic switches are required to connect one of two matching circuits to the coils at the proper time. Most often, PIN diodes are used for switching the matching circuits at radio frequencies. Fig. 13 shows the simulation result. In this figure, first, we used two identical matching circuits for edge coils and another matching circuit for the central one to match them at 121 MHz, where $S_{11} = S_{33} \approx -85$, $S_{22} \approx -35$, $S_{12} = S_{21} = S_{23} = S_{32} = -18$ dB, and $S_{13} = S_{31} \approx -37$ (shown in the frequency range 100–180 MHz); then, we used another two matching circuits again for edge coils and another matching circuit for the central one to match them at 298 MHz. At this band, $S_{11} = S_{33} \approx -70$, $S_{22} \approx -100$, $S_{12} = S_{21} = S_{23} = S_{32} = -42$ dB, and $S_{13} = S_{31} \approx -67$ (shown in the frequency range

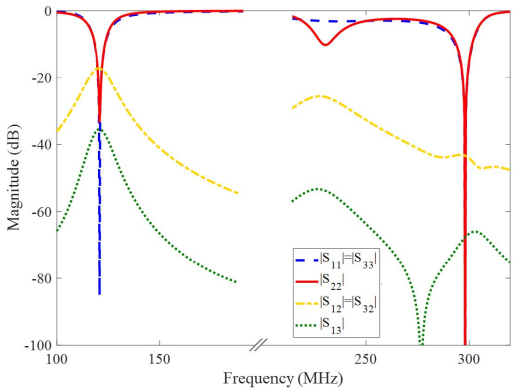

Fig. 13. S-parameters of three TRHICs separated by 3 cm gap located 1 cm above a cubic phantom with $\epsilon_r = 40$. For each band, a separate matching circuit is connected to each coil for both S_{ii} and S_{ij} calculations. The result of using matching circuits for the first band is shown in the frequency range of 100–180 MHz, and the result of using other matching circuits for the second band is shown in the frequency range of 220–320 MHz.

220–320 MHz). These results demonstrate the possibility of decoupling at both bands simultaneously in the presence of a human body. Experimental verification will be done in the next stage of the research.

VI. Conclusion

A method for designing self-decoupled dual-band transceiver HICs has been suggested. By adding two asymmetric gaps to the shield of a cable loop and optimizing the positions of these gaps, we may tune two resonance frequencies separately. We have applied our approach so that to develop a TRHIC for scanning phosphor and hydrogen in UHF (7 T) MRI scanners. In the receiving regime, the performance of our antenna is almost the same as that of previously reported HICs with an only difference: now, this operation is engineered in two bands. The decoupling in the transmission regime in the first band is achieved by overlapping the neighboring TRHICs, whereas the antenna ports are located in the opposite extremities of the loops (decoupling was possible even without rotation of the second coil at this band). The same alternating location of the antenna ports allows us to decouple the TRHICs in the transmitting regime in the second band. Here, we utilized the second hybrid mode of the TRHIC, engineered so that the electric and magnetic dipole components are balanced. To verify our theory for the transmitting regime, we: 1) numerically calculated and measured the resonance frequencies that we have engineered, 2) calculated and measured the Z matrix of the array of two TRHICs, 3) studied theoretically and experimentally the coupling in the array of two TRHICs, and 4) did the same for the array of three TRHICs. Also, we have numerically checked the concept of the balanced mode in the second band and the negligibility of the induced current in reception at both bands. As mentioned above, the overlapping of the coils and their rotations are not advantageous when either there are more than two coils or mechanical movement, e.g., patient comfort, is requested. It is technically unsuitable for imaging small and closely located human organs and human body parts, such as fingers [11], [12]. For these applications, we may consider the design of the array with the positive $d \geq 1$ cm as a practical design. The coupling in the transmitting regime at the second frequency is very weak even for an array of TRHICs located in free space. In the presence of the human body, the coupling at this frequency will obviously decrease once more. As to the first working frequency, for an array of non-overlapped coils located in free space, the coupling at the first frequency is below -8 dB only in reception. In the transmitting regime, the coupling coefficient of the adjacent coils in such an array at 121 MHz is higher. However, our simulations show that, in the presence of the human body, it decreases to $S_{12} \leq -18$ dB, and practical implementation of an arrayed dual-band TRHIC for imaging the small and closely located organs is possible. This issue will be experimentally studied in the next stage of our research.

References

[1] W. Mao, M. B. Smith, and C. M. Collins, "Exploring the limits of RF shimming for high-field MRI of the human head," *Magn. Reson. Med.*, vol. 56, no. 4, pp. 918–922, Oct. 2006.

[2] T. S. Ibrahim and L. Tang, "Insight into RF power requirements and B1 field homogeneity for human MRI via rigorous FDTD approach," *J. Magn. Reson. Imag.*, vol. 25, no. 6, pp. 1235–1247, Jun. 2007.

[3] N. I. Avdievich, J. W. Pan, and H. P. Hetherington, "Resonant inductive decoupling (RID) for transceiver arrays to compensate for both reactive and resistive components of the mutual impedance," *NMR Biomed.*, vol. 26, no. 11, pp. 1547–1554, Nov. 2013.

[4] P. B. Roemer, W. A. Edelstein, C. E. Hayes, S. P. Souza, and O. M. Müeller, "The NMR phased array," *Magn. Reson. Med.*, vol. 16, no. 2, pp. 192–225, 1990.

[5] A. J. Fenn, *Adaptive Antennas Phased Arrays for Radar Communication*. London, U.K.: Artech House, 2008.

[6] M. S. M. Mollaei, A. Hurshkainen, S. Kurdjumov, S. Glybovski, and C. Simovski, "Passive electromagnetic decoupling in an active metasurface of dipoles," *Photon. Nanostruct. Fundam. Appl.*, vol. 32, pp. 53–61, Dec. 2018.

[7] A. Hurshkainen *et al.*, "Decoupling of closely spaced dipole antennas for ultrahigh field MRI with metasurfaces," *IEEE Trans. Antennas Propag.*, vol. 69, no. 2, pp. 1094–1106, Feb. 2021.

[8] X. Yan, X. Zhang, B. Feng, C. Ma, L. Wei, and R. Xue, "7T transmit/receive arrays using ICE decoupling for human head MR imaging," *IEEE Trans. Med. Imag.*, vol. 33, no. 9, pp. 1781–1787, Sep. 2014.

[9] I. R. O. Connell, K. M. Gilbert, M. A. Abou-Khousa, and R. S. Menon, "Design of a parallel transmit head coil at 7T with magnetic wall distributed filters," *IEEE Trans. Med. Imag.*, vol. 34, no. 4, pp. 836–845, Apr. 2015.

[10] X. Yan, J. C. Gore, and W. A. Grissom, "Self-decoupled radiofrequency coils for magnetic resonance imaging," *Nature Commun.*, vol. 9, no. 1, P. 3481, Aug. 2018.

[11] B. Zhang, D. K. Sodickson, and M. A. Cloos, "A high-impedance detector-array glove for magnetic resonance imaging of the hand," *Nature Biomed. Eng.*, vol. 2, no. 8, pp. 570–577, May 2018.

[12] T. Ruytenberg, A. Webb, and I. Zivkovic, "Shielded-coaxial-cable coils as receive and transceive array elements for 7T human MRI," *Magn. Reson. Med.*, vol. 83, no. 3, pp. 1135–1146, Mar. 2020.

[13] M. S. M. Mollaei, C. C. Van Leeuwen, A. J. E. Raaijmakers, and C. R. Simovski, "Analysis of high impedance coils both in transmission and reception regimes," *IEEE Access*, vol. 8, pp. 129754–129762, 2020.

[14] E. Laistler and E. Moser, "Handy magnetic resonance coils," *Nature Biomed. Eng.*, vol. 2, no. 8, pp. 557–558, Aug. 2018.

[15] R. Frass-Kriegl *et al.*, "Multi-turn multi-gap transmission line resonators—Concept, design and first implementation at 4.7 T and 7 T," *J. Magn. Reson.*, vol. 273, pp. 65–72, Dec. 2016.

[16] L. Nohava *et al.*, "Flexible multi-turn multi-gap coaxial RF coils: Design concept and implementation for magnetic resonance imaging at 3 and 7 Tesla," *IEEE Trans. Med. Imag.*, vol. 40, no. 4, pp. 1267–1278, Apr. 2021.

[17] M. Obermann *et al.*, "Ultra-flexible and light-weight 3-channel coaxial transmission line resonator receive-only coil array for 3T," in *Proc. Intl. Soc. Mag. Reson. Med.*, vol. 27, p. 1558, Mar. 2014.

Masoud Sharifian Mazraeh Mollaei was born in Tehran, Iran, in 1989. He received the B.Sc. degree in electrical engineering from Imam Khomeyni Internationa University, Qazvin, Iran, in 2013, and the M.Sc. degree in electrical engineering from Iran University of Science and Technology (IUST), Tehran, Iran, in 2016. He is currently pursuing the Ph.D. degree with the Department of Electronics and Nanotechnology, Aalto University, Espoo, Finland, where he has been developing theoretical ad experimental techniques for ultrahigh field magnetic resonance imaging.

His current research interests include array antenna, antenna decoupling, metamaterials, and photonics. The aim of his thesis is to introduce a novel method for decoupling dipole and loop antenna arrays for 7 T MRI.

Ali Sharifian Mazraeh Mollaei was born in Tehran, Iran, in 1991. He received the B.Sc. degree in electrical engineering from Imam Khomeyni Internationa University, Qazvin, Iran, in 2014, and the M.Sc. degree in electrical engineering from the University of Tehran, Tehran, in 2019.

His current research interests include channel coding, image processing, and array antenna.

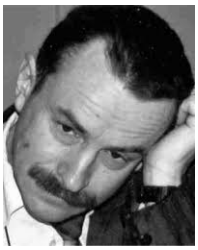

Constantin R. Simovski was born in Saint Petersburg, Russia, in December 1957. He received the Dipl.-Eng. degree (by Research) in radio engineering, the Ph.D. degree in electromagnetic theory, and the D.Sc. degree from Saint Petersburg State Polytechnic University (formerly Leningrad Polytechnic Institute, and State Technical University), Saint Petersburg, in 1980, 1986, and 2000, respectively.

From 1980 to 1992, he was with the Soviet scientific and industrial firm "Impulse," Saint Petersburg, Russia. In 1986, he defended the Candidate of Science (Ph.D.) thesis (a study of the scattering of Earth waves in the mountains) at Leningrad Polytechnic Institute. In 1992, he joined Saint Petersburg University of Information Technologies, Mechanics and Optics, as an Assistant, where, from 1994 to 1995, he was an Assistant Professor, from 1995 to 2001, he was an Associate Professor, and, since 2001, he has been a Full Professor. In 2000, he defended the D.Sc. thesis (a theory of 2-D and 3-D bianisotropic scattering arrays). Since 1999, he has been involved in the theory and applications of 2-D and 3-D electromagnetic band-gap structures for microwave and ultrashortwave antennas. His current research interests include metamaterials for microwave and optical applications, including optics of metal nanoparticles.